Visualization of Principal Curvature Directions by Anisotropic Diffusion

U. Diewald, M. Rumpf

Institute for Applied Mathematics, University of Bonn, Wegelerstraße 6, 53115 Bonn, Germany
[*diewald* | *rumpf*]*@iam.uni-bonn.de*

Abstract

Anisotropic diffusion is known to be a powerful tool in image processing. It enables the smoothing of initially noisy images while still retaining, respectively sharpening edges and enhancing features. Here recent results in the context of vector field visualization are expanded to non Euclidean domains. The aim is to graphically represent vector field data on two dimensional surfaces in an intuitively understandable way. Furthermore the multiscale properties of the approach support a scale of resolutions, ranging from detailed flow representation to a coarse overview of field data. Here an initial noisy image intensity is smoothed along integral lines, whereas the image is mainly sharpened in the orthogonal direction. The method is based on a continuous model and requires the solution of a parabolic PDE problem on manifolds. It is discretized by finite elements on surface triangulations only in the final implementational step. Applications are shown for principal directions of curvature on general surfaces.

1 Introduction

The visualization of vector field data, especially of velocity fields from CFD computations is one of the fundamental tasks in scientific visualization. Such fields are often given on curved domains, especially surfaces embedded in $\mathbb{R}^3$. Examples are meteorological flow fields on the sphere or the sheer flow on the boundary of a moving body. Furthermore, geometric vector fields such as the principal directions of curvature or other eigenvector fields are important quantities of interest (cf. Fig. 1).

Figure 1: The principal directions of curvature are shown by some texture on a torus.

A variety of different approaches has been presented. The simplest method to draw vector plots at nodes of some overlaying grid in general produces visual clutter, because of the typically different local scaling of the field in the spatial domain, which leads to disturbing multiple overlaps in certain regions, whereas in other areas small structures such as eddies can not be resolved adequately. This gets even worse if tangential fields on highly curved surfaces are considered. In addition the selection of “regularly“ distributed sample points on a curved surface which is not described by a single map is already a difficult task.

Thus, the central goal is to come up with an intuitively better receptible method, which gives an overall as well as detailed view of the flow pattern. Single particle lines only very partially enlighten features of a complex flow field. Instead, we ask for a texture representing a vector field on a surfaces. Here we confine ourselves to stationary fields on a manifold $\mathcal{M}$ embedded in

$\mathbb{R}^3$ and consider a tangential vector field v.

Nowadays already a classical approach is the spot noise method proposed by van Wijk [22] and improved by de Leeuw and Van Wijk [6]. It introduces spot like texture splats on the domain which are aligned by deformation to the velocity field in 2D or on surfaces in 3D. These splats are plotted on the fluid domain showing strong alignment patterns in the flow direction. The Line Integral Convolution (LIC) approach of Cabral and Leedom [3] integrates the fundamental ODE describing streamlines forward and backward in time at every pixelized point in the domain, convolves a white noise along these particle paths with some Gaussian type filter kernel, and takes the resulting value as an intensity value for the corresponding pixel. This method was improved by Hege and Stalling [20] especially by reusing portions of the convolution integral already computed on points along the streamline. Forssell [11] proposed a similar method on surfaces and Max et al. [15] discuss flow visualization by texturing on contour surfaces. Max and Becker [14] presented a method for visualizing 2D and 3D flows by animating textures. In [2] Lagrangian coordinates calculated by some finite volume scheme on the computational domain are applied for the texturing of the computational domain according to a timedependent flow field.
Shen and Kao [19] applied a LIC type method to unsteady flow fields. Interrante and Grosch [12] generalized line integral convolution to 3D in terms of volume rendering of line filaments.

Most of the methods presented so far have in common, that the generation of a coarser scale requires a new computation. For instance, if we ask for a finer or coarser scale of the line integral convolution pattern, the computation has to be restarted with a coarser initial image intensity. In case of spot noise larger spots have to be selected and their stretching along the field has to be increased.

Recently [18] a new approach based on image processing methodology using nonlinear diffusion has been presented which also generates stretched streamline type patterns on an Euclidean domain and incorporates a successive coarsening as time proceeds in the underlying diffusion problem. Methods, which are based on such a scale of spaces and enhance certain structures of images have become popular in image processing analysis since in ‘87 Perona and Malik [16] proposed a first continuous diffusion model which allows the denoising of images together with the enhancing of edges. Catté et al. [4] discussed a regularization method where the diffusion coefficient is no longer evaluated on the exact intensity gradient. The recovering of lower dimensional structures in images is analyzed by Weickert [23], who introduced an anisotropic nonlinear diffusion method where the diffusion matrix depends on the so called structure tensor of the image. Concerning the numerical implementation Weickert proposed finite difference schemes [23] and Kačur and Mikula [13] suggested a semi-implicit finite element implementation for the isotropic model by Catté et al.. Large stencils have to be considered in case of the implementation of anisotropic diffusion by finite differences. This is a crucial shortcoming of such methods, especially if we consider a geometric counterpart on discrete surfaces. In [17] an adaptive finite element method is discussed in 2D and 3D for image processing by anisotropic nonlinear diffusion.

Here we will briefly review the basic concepts of the nonlinear diffusion method on Euclidean domains described in [18]. Then we will carry over this method to surfaces making use of classical differential calculus on surfaces.

For some background information on geometry we refer to the general introduction to differential calculus on manifolds in the book by do Carmo [8]. Furthermore let us mention that our discretization approach is mainly motivated by the work of Dziuk [9], who presented this type of finite element algorithm for the solution of partial differential equations on surfaces. Furthermore in [10] he discusses a numerical method for geometric diffusion applied to the surface itself, which coincides with the mean curvature motion.

2 Reviewing the anisotropic diffusion method on Euclidean domains

Here, we confine ourselves to the case of planar domains in 2D. Nonlinear anisotropic diffusion applied to some initial random noisy image will enable an intuitive and scalable visualization of complicated vector fields. Therefore, we have picked up the idea of line integral convolution, where a strong correlation of the image intensity along integral lines is achieved by convolution of an initial white noise along these lines. If we ask for a well posed continuous diffusion problem with similar properties, we are lead to some anisotropic diffusion, now controlled by a suitable diffusion matrix.

We consider the parabolic boundary and initial value problem and ask for a function $\rho : \mathbb{R}_0^+ \times \Omega \to \mathbb{R}$ which solves

$$\begin{aligned} \frac{\partial}{\partial t}\rho - \operatorname{div}(A\nabla\rho) &= f(\rho) \text{ in } \mathbb{R}^+ \times \Omega\,, \\ \rho(0,\cdot) &= \rho_0 \text{ on } \Omega\,, \\ \frac{\partial}{\partial \nu}\rho &= 0 \text{ on } \mathbb{R}^+ \times \partial\Omega \end{aligned}$$

for given initial density $\rho_0 : \Omega \to [0,1]$. Here $\rho_\epsilon = \chi_\epsilon * \rho$ is a mollification of the current density (cf. Catté et al. [4]). We interpret the density as an image intensity, a scalar greyscale or – with a slight extension to the vector valued case – as a vector valued color. Thus, the solution $\rho(\cdot)$ can be regarded as a family of images or textures $\{\rho(t)\}_{t\in\mathbb{R}_0^+}$, where the time t serves as a scaling parameter.

Now we consider the anisotropic diffusion matrix A. For a given vector field $v : \Omega \to \mathbb{R}^2$ we take into account linear diffusion in the direction of the vector field and a Perona Malik type diffusion orthogonal to the field. Let us suppose that v is continuous and $v \neq 0$ on Ω. Then there exists a family of continuous orthogonal mappings $B(v) : \Omega \to SO(2)$ such that $B(v)v = \|v\|e_0$, where $\{e_i\}_{i=0,\cdots,n-1}$ is the standard base in $\mathbb{R}^n$. Hence, we define $A = A(v, \nabla\rho_\epsilon)$ with

$$A(v,d) = B(v)^T \begin{pmatrix} \alpha(\|v\|) & \\ & G(d) \end{pmatrix} B(v)$$

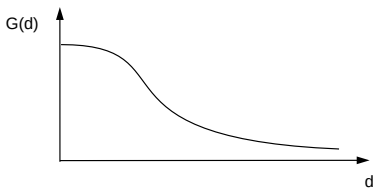

Figure 2: The shape $G(\cdot)$ which applied to the gradient of the mollified image intensity serves as a diffusion coefficient in image processing.

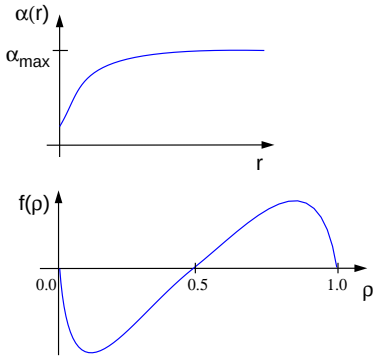

Figure 3: The graphs of the velocity dependent linear diffusion $\alpha(\cdot)$, respectively the scalar contrast enhancing right hand side $f(\cdot)$.

where $\alpha : \mathbb{R}^+ \to \mathbb{R}^+$ controls the linear diffusion in vector field direction, i. e. along streamlines, and the diffusion coefficient $G(d) = \frac{\beta}{1+\|d\|^2}$ (cf. Fig. 2) acts in the orthogonal direction and is responsible for the image sharpening in the cross streamline direction. We may either choose a linear function α or in case of a velocity field, which spatially varies over several orders of magnitude, we select a monotone function α (cf. Fig. 3) with $\alpha(0) > 0$ and $\lim_{s\to\infty}\alpha(s) = \alpha_{\max}$. As initial data ρ_0 we choose some random noise of an appropriate frequency range. This can for instance be generated running a linear isotropic diffusion simulation on a discrete white noise for a short time. Hence patterns will grow upstream and downstream, whereas the edges tangential to these patterns are successively enhanced. Still there is some diffusion perpendicular to the field, which supplies us for evolving time with a scale of progressively coarser representation of the flow field. Finally, the image contrast has to be strengthened during the evolution. This is achieved selecting an appropriate function $f : [0,1] \to \mathbb{R}^+$

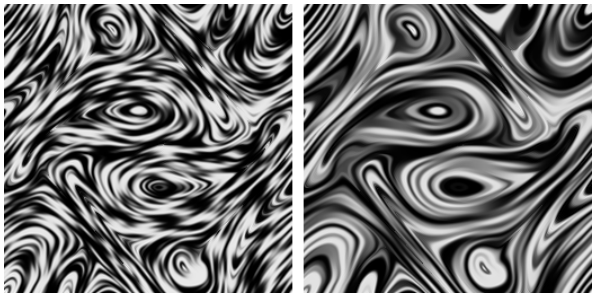

Figure 4: A vector field from a 2D magneto-hydrodynamics simulation (MHD) is visualized by nonlinear diffusion. A discrete white noise is considered as initial data. We run the evolution on the left for a small and on the right for a large constant diffusion coefficient α.

(cf. Fig. 3) with $f(0) = f(1) = 0$ and $f > 0$ on $(0.5, 1)$, and $f < 0$ on $(0, 0.5)$. Finally we end up with the method of nonlinear anisotropic diffusion already presented in [18] to visualize complex vector fields (cf. Fig. 4). The set of pointwise asymptotic limits of the evolution is $\{0, 1\}$ due to the choice of the contrast enhancing function $f(\cdot)$. Analytically 0.5 is a third, but unstable fix point of the dynamics. This set and the induced richness of the resulting texture can be increased studying a vector valued intensity $\rho : \Omega \to [0, 1]^m$ for some $m \geq 1$ and a corresponding system of parabolic equations. The equations are coupled solely by the nonlinear diffusion coefficient $G(\cdot)$ (which now depends on the norm $\|\nabla\rho\|$ of the Jacobian of the vector valued density $\nabla\rho$) and the right hand side $f(\cdot)$. We define $f(\rho) = h(\|\rho\|)\rho$ with $h(s) = \tilde{f}(s)/s$ for $s \neq 0$, where $\tilde{f}$ is the old right hand side from the scalar case, and $h(0) = 0$. Furthermore we select an initial density which is now a discrete "white noise with values in $B_1(0) \cap [0, 1]^m$. Thus the contrast enhancing now pushes the pointwise vector density ρ either to the 0 or to some value on the sphere sector $S^{m-1} \cap [0, 1]^m$ in $\mathbb{R}^m$.

3 Anisotropic diffusion on surfaces

Above we have discussed anisotropic diffusion in vector field visualization on domains which are subsets of two- and three dimensional Euclidian space. Now we will outline how to carry over this methodology to display tangential vector fields on surfaces. Important examples are results from meteorological simulations, flow fields on streamsurfaces, or vector fields in differential geometry. Based on the well established intrinsic differential calculus on manifolds [8], we can pick up the same diffusion problems with an appropriate reinterpretation of the operators. Thus, let us first briefly review the basic notation of manifolds, differential calculus and geometric diffusion. For a detailed introduction to geometry and differential calculus we refer to [8] and [5, Chapter 1]. For the sake of simplicity we assume our surfaces to be compact embedded manifolds without boundary. In case of bounded manifolds we lateron have to take into account natural boundary conditions as in the Euclidean case. Thus we consider a smooth manifold $\mathcal{M}$, which we suppose to be embedded in $\mathbb{R}^3$. Let $x : \Omega \to \mathcal{M}\,; \xi \mapsto x(\xi)$ be a coordinate map from an atlas of $\mathcal{M}$. For each point x on $\mathcal{M}$ the embedded tangent space $\mathcal{T}_x\mathcal{M}$ is spanned by the basis $\{\frac{\partial x}{\partial \xi_1}, \frac{\partial x}{\partial \xi_2}\}$. By $\mathcal{TM}$ we denote the tangent bundle. On $\mathcal{M}$ the metric $g(\cdot, \cdot)$ as a bilinear form on $\mathcal{TM} \times \mathcal{TM}$ is prescribed by the metric tensor $g = (g_{ij})_{ij}$ with

$$g_{ij} = \frac{\partial x}{\partial \xi_i} \cdot \frac{\partial x}{\partial \xi_j} \,,$$

where $\cdot$ indicates the scalar product in $\mathbb{R}^3$. The inverse of g is denoted by $g^{-1} = (g^{ij})_{ij}$. Based on the metric we can define the integration of a function f on $\mathcal{M}$. We split up an integral over $\mathcal{M}$ into separate integrals over subsets, which are in the image $x(\Omega)$ of some coordinate map x and define

$$\int_{x(\Omega)} f := \int_\Omega f(x(\xi)) \sqrt{\det g}\, \mathrm{d}\xi \,.$$

Integrating either a product of two functions f, g on $\mathcal{M}$ or the product of two vector fields v, w on $\mathcal{TM}$ we obtain the following scalar products on

$C^0(\mathcal{M})$ and $C^0(\mathcal{TM})$, respectively:

$$\begin{aligned}(f,g)_{\mathcal{M}} &:= \int\limits_{\mathcal{M}} fg \ \mathrm{d}x \ , \\ (v,w)_{\mathcal{TM}} &:= \int\limits_{\mathcal{M}} g(v,w) \ \mathrm{d}x \ .\end{aligned}$$

Next, we have to introduce the fundamental intrinsic gradient and divergence operators on $\mathcal{M}$. The gradient $\nabla_{\mathcal{M}} f$ of f is defined as the representation of df with respect to the metric g. We obtain in coordinates

$$\nabla_{\mathcal{M}} f = \sum_{i,j} g^{ij} \frac{\partial (f \circ x)}{\partial \xi_j} \frac{\partial x}{\partial \xi_i} \ .$$

Furthermore, we define the divergence $\mathrm{div}_{\mathcal{M}} v$ for a vector field $v \in \mathcal{TM}$ as the dual operator of the negative gradient by

$$\int\limits_{\mathcal{M}} \mathrm{div}_{\mathcal{M}} v \ \phi \ \mathrm{d}x := - \int\limits_{\mathcal{M}} g(v, \nabla_{\mathcal{M}} \phi) \ \mathrm{d}x$$

for all $\phi \in C_0^\infty(\mathcal{M})$.

Finally, with these differential operators at hand we can discuss a general and intrinsic diffusion on a manifold in analogy to diffusion in Euclidean space: We ask for a solution $\rho : \mathbb{R}_0^+ \times \mathcal{M} \to \mathbb{R}$ of the parabolic equation

$$\frac{\partial}{\partial t} \rho - \mathrm{div}_{\mathcal{M}} (A \nabla_{\mathcal{M}} \rho) = f(\rho)$$

on $\mathbb{R}_0^+ \times \mathcal{M}$ for given initial data $\rho(0, \cdot\,) = \rho_0$ on $\mathcal{M}$. Here we suppose A to be some positive definite symmetric endomorphism on $\mathcal{TM}$. Testing with any function $\theta \in C^\infty(\mathcal{M}(t))$ and integrating over $\mathcal{M}$ we obtain the variational formulation

$$(\partial_t \rho, \theta)_{\mathcal{M}} + (A \nabla_{\mathcal{M}} \rho, \nabla_{\mathcal{M}} \theta)_{\mathcal{TM}} = (f(\rho), \theta)_{\mathcal{M}} \ .$$

Lateron, we will recall this in case of a suitable finite element implementation. Now we consider our actual goal, which is the generation of a texture by nonlinear anisotropic diffusion to represent a given vector field $v \in \mathcal{TM}$ on the surface. Thus, we suppose A to depend on the vector field v and the norm of the geometric gradient of a convoluted intensity ρ_ϵ:

$$A = A(v, \|\nabla_{\mathcal{M}} \rho_\epsilon\|)$$

For non vanishing v let $w \in \mathcal{T}_x\mathcal{M}$ be some unit vector normal to v, i. e. $g(v,w) = 0$. Hence, $\{\frac{v}{\|v\|}, w\}$ is a basis of $\mathcal{T}_x\mathcal{M}$ and with respect to this basis we define as before in the Euclidean case

$$A(v,d) = \begin{pmatrix} \alpha(\|v\|) & \\ & G(d) \end{pmatrix} \ .$$

As right hand side $f(\cdot)$ we pick up the one already introduced in Section 2 and again assume ρ_0 to be a random noise, either scalar or vector valued, but now prescribed on the surface $\mathcal{M}$. Furthermore, we have to give a suitable definition of the regularizing presmoothing to obtain ρ_ϵ from the original intensity ρ.

In the Euclidean case Kačur and Mikula [13] proposed a convolution with the heat equation kernel for the regularization of the problem. I.e. if one defines $\rho_\epsilon = \tilde{\rho}(t = \epsilon^2/2)$ where $\tilde{\rho}$ is the solution of the heat equation with initial data ρ, then ϵ is the width of the corresponding Gaussian filter.

Again, we proceed in analogy to the Euclidian case and define ρ_ϵ as the result of the above diffusion problem with $A = \mathrm{Id}$ at time $t = \frac{\epsilon^2}{2}$ and for initial data ρ.

Finally, the resulting family $\{\rho(t)\}_{t \geq 0}$ of intensities on $\mathcal{M}$ gives a multiscale of representations of the given vector field v. Figure 5,6,7 show results on different surfaces. We consider the principal directions of curvature as tangential vector fields on which we apply the anisotropic diffusion method. On the underlying triangular grids, the shape operator, whose eigenvalues are the principal curvatures, is approximated as follows. Locally we regard a single triangle T and all the neighboring triangles which have a non zero intersection with T as a graph over the plane containing T. Next, we calculate the L^2 projection of this piecewise linear graph onto the set of quadratic graphs which are tangential to the plane. Then we evaluate the constant shape operator on this graph. Let us emphasize that the L^2 projection is always defined, although the local graph property of the triangular grid might not hold in certain degenerate cases. For details we refer to [7].

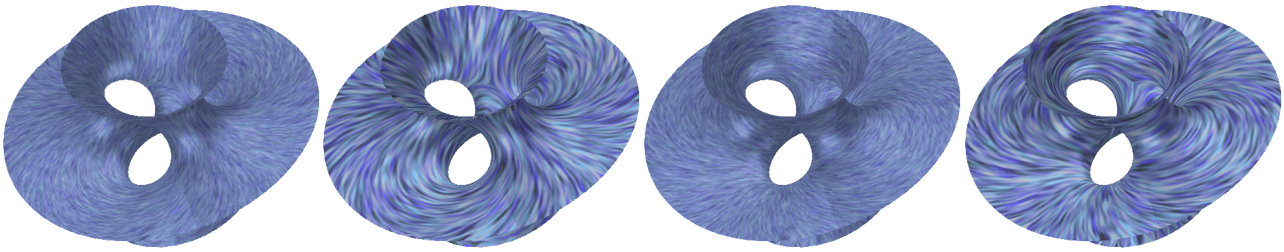

Figure 5: The principal directions of curvature are visualized by anisotropic diffusion on a minimal surface.

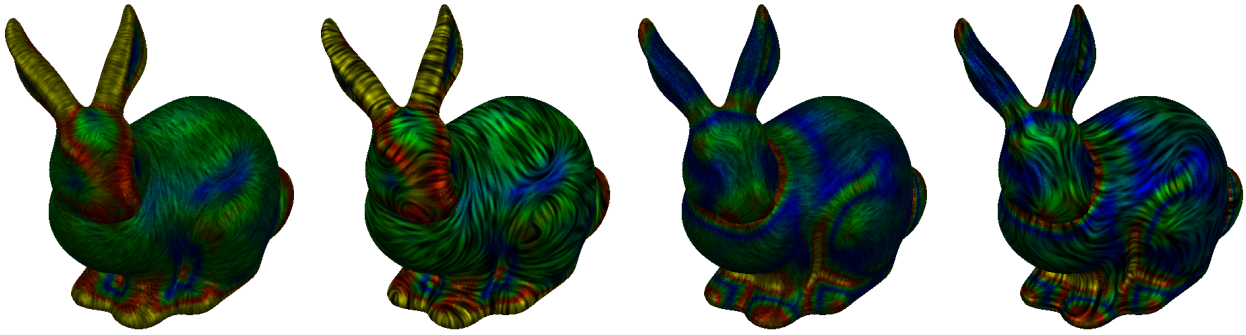

Figure 6: For both principal directions of curvature different timesteps of the anisotropic diffusion are displayed on the surface of a presmoothed Stanford bunny. In addition the corresponding principal curvature values are color coded.

Figure 7: Two timesteps of the anisotropic diffusion on a presmoothed venus data set are shown.

4 Finite element discretization

In what follows we discuss the discretization and implementation of the field aligned diffusion method on surfaces. For this purpose a finite element discretization in space and a semi implicit backward Euler or second order Crank Nicolsson scheme in time are considered. We suppose the surface $\mathcal{M}$ to be approximated with a sufficiently fine triangular grid $\mathcal{M}_h$ consisting of nondegenerate triangles T with maximal diameter h. By sufficiently we especially mean, that the original grid might be further refined to ensure an appropriate resolution of the flow field by means of the proposed method. On the triangulation we consider the standard linear finite element space. Numerical integration is based on the lumped masses product $(\cdot,\cdot)^h_{M_h}$ [21] for the L^2 product $(\cdot,\cdot)_{M_h}$ in the variational formulation and a one point quadrature rule for the bilinear form $(A\nabla_{\mathcal{M}}\cdot,\nabla_{\mathcal{M}}\cdot)_{\mathcal{TM}}$. Semi implicit means for the schemes considered here that the nonlinearity $A(\cdot)$ is evaluated at the old time. Finally, in each step of the discrete evolution we have to solve a single system of linear equations. We obtain for a backward Euler discretization

$$(M^k + \tau L^k(A^k))\bar{\rho}^{k+1} = M^k\bar{\rho}^k + \tau M^k\bar{f}^k\,.$$

Here $\bar{\rho}^k = (\bar{\rho}^k_i)_i$ is the vector of nodal intensity values at time $t^k = k\tau$, where τ is the selected time step size. Furthermore, if we denote the "hat shaped" basis functions by Φ_i and the diffusion tensor with respect to the discrete intensity at time t^k by A^k,

$$\begin{aligned} M^k &:= \left((\Phi_i,\Phi_j)^h_{M_h}\right)_{ij} \\ L^k(A^k) &:= \left((A^k\nabla_{\mathcal{M}_h}\Phi_i, \nabla_{\mathcal{M}_h}\Phi_j)_{M_h}\right)_{ij} \end{aligned}$$

are the lumped mass matrix and nonlinear stiffness matrix, respectively. Finally, the components of the right hand side $\bar{f}^k$ are evaluated by $(\bar{f}^k)_i = f(\bar{\rho}^k_i)$.

The global matrices M^k and $L^k(A^k)$ are assembled from local matrices m^T and l^T with respect to a single triangle T. Their entries correspond to all pairings of local basis functions. Compared to the method on Euclidean domains the algorithm is completely identical up to evaluation of these local matrix entries. Thus, we now focus on them. We obtain by lumped mass integration

$$m^T_{ij} = \frac{1}{3}\delta_{ij}|T|$$

where $|T|$ is the area of the triangle T. Next, let us consider for every triangle T the reference triangle $\hat{T}\subset\mathbb{R}^2$ with independent variables ξ_1,ξ_2 and nodes $\xi^0=(0,0)$, $\xi^1=(1,0)$, and $\xi^2=(0,1)$. Then an affine coordinate mapping X maps $\hat{T}$ onto T and its nodes ξ^i onto the corresponding nodes P^i of T on the discrete surface in $\mathbb{R}^3$. Hence the corresponding metric tensor is as in the continuous case given by $g_{ij} = \frac{\partial X}{\partial\xi_i}\cdot\frac{\partial X}{\partial\xi_j}$, where $\frac{\partial X_k}{\partial\xi_i} = P^i_k - P^0_k$. Hence we can evaluate gradients of the linear basis functions Φ^l corresponding to the nodes P^l by

$$\nabla_{\mathcal{M}_h}\Phi^l = \sum_{i,j} g^{ij}\frac{\partial\Phi^l}{\partial\xi_j}(P^i - P^0)\,,$$

where the derivatives of Φ^l with respect to the reference coordinates ξ are

$$\begin{pmatrix} \frac{\partial\Phi^l}{\partial\xi_1} \\ \frac{\partial\Phi^l}{\partial\xi_2} \end{pmatrix} = \begin{pmatrix} -1 \\ -1 \end{pmatrix}, \begin{pmatrix} 1 \\ 0 \end{pmatrix}, \begin{pmatrix} 0 \\ 1 \end{pmatrix}\,.$$

Finally we calculate the local nonlinear stiffness matrix

$$\begin{aligned} &l^T_{ij}(A) = \\ &|T|\left[\alpha(\|V\|)\left(\nabla_{\mathcal{M}_h}\Phi^i\cdot\frac{V}{\|V\|}\right)\left(\nabla_{\mathcal{M}_h}\Phi^j\cdot\frac{V}{\|V\|}\right) + \right. \\ &\qquad G(D)\left(\nabla_{\mathcal{M}_h}\Phi^i - \nabla_{\mathcal{M}_h}\Phi^i\cdot\frac{V}{\|V\|^2}V\right) \\ &\qquad\left.\cdot\left(\nabla_{\mathcal{M}_h}\Phi^j - \nabla_{\mathcal{M}_h}\Phi^j\cdot\frac{V}{\|V\|^2}V\right)\right]\,. \end{aligned}$$

where $V = v(c_T)$ for the center of mass c_T of T, D the geometric gradient of the presmoothed discrete intensity on T and "$\cdot$" still indicates the scalar product in $\mathbb{R}^3$.

Finally, in each timestep the computation of the prefiltered intensity vector $\bar{\rho}^n_\epsilon$ is based on a single implicit time step $\epsilon^2/2$ for the corresponding discrete heat equation scheme with respect to initial data $\bar{\rho}^n$.

5 Conclusions

We have expanded a method [18, 1] based on the solution of a nonlinear anisotropic diffusion problem for the post processing of vector data to the case on non Euclidean domains. With the original method the current expansion shares several advantages. Especially it is well founded on a physically intuitive continuous model and its discretization in the final step is along the approved guidelines of finite element calculus.

Furthermore the current approach is characterized by the very natural carrying over of the approach from the Euclidean case to the case of curved surfaces. Thus given a triangulation, which is the standard representation of surfaces also in computer graphics, the proposed method is straightforward to implement. From the authors' point of view exciting future research directions are a further exploration of adaptive finite element paradigms to improve the methods performance. Furthermore, algebraic multigrid methods may help to reduce the cost in the solution of the linear problems for each timestep. Finally, an anisotropic diffusion flow segmentation as proposed in [18] on 2D domains also carries provisions for the identification of interesting flow regions on surfaces.

Acknowledgement

The authors would like to acknowledge Ulrich Clarenz for inspiring discussions on geometric calculus. Furthermore they thank Konrad Polthier from the Technical University at Berlin and Wolfram Rosenbaum from Bonn for providing the minimal surface data and the MHD simulation data sets.

References

[1] J. Becker, T. Preußer, and M. Rumpf. Pde methods in flow simulation post processing. *Computing and Visualization in Science, to appear*, 1999.

[2] J. Becker and M. Rumpf. Visualization of time-dependent velocity fields by texture transport. In *Proceedings of the Eurographics Scientific Visualization Workshop '98*. Springer, 1998.

[3] B. Cabral and L. Leedom. Imaging vector fields using line integral convolution. In J. T. Kajiya, editor, *Computer Graphics (SIGGRAPH '93 Proceedings)*, volume 27, pages 263–272, Aug. 1993.

[4] F. Catté, P. L. Lions, J. M. Morel, and T. Coll. Image selective smoothing and edge detection by nonlinear diffusion. *SIAM J. Numer. Anal.*, 29:182–193, 1992.

[5] I. Chavel. *Eigenvalues in Riemannian Geometry*. Academic Press, 1984.

[6] W. C. de Leeuw and J. J. van Wijk. Enhanced spot noise for vector field visualization. In *Proceedings Visualization '95*, 1995.

[7] U. Diewald, U. Clarenz, and M. Rumpf. Nonlinear anisotropic diffusion in surface processing. Submitted for publication, 2000.

[8] M. P. do Carmo. *Riemannian Geometry*. Birkhäuser, Boston–Basel–Berlin, 1993.

[9] G. Dziuk. Finite elements for the beltrami operator on arbitrary surfaces. In *Partial differential equations and calculus of variations, Lect. Notes Math. 1357*, 1988.

[10] G. Dziuk. An algorithm for evolutionary surfaces. *Numer. Math.*, 58:603–611, 1991.

[11] L. Forssell. Visualizing flow over curvilinear grid surfaces using line integral convolution. In *Proceedings IEEE Visualization '94*, pages 240–246, 1994.

[12] V. Interrante and C. Grosch. Stragegies for effectively visualizing 3d flow with volume lic. In *Proceedings Visualization '97*, pages 285–292, 1997.

[13] J. Kačur and K. Mikula. Solution of nonlinear diffusion appearing in image smoothing and edge detection. *Appl. Numer. Math.*, 17 (1):47–59, 1995.

[14] N. Max and B. Becker. Flow visualization using moving textures. In *Proceedings of the ICASE/LaRC Symposium on Time Varying Data, NASA Conference Publication 3321*, pages 77–87, 1996.

[15] N. Max, R. Crawfis, and C. Grant. Visualizing 3D Velocity Fields Near Contour Sur-

face. In *Proceedings of IEEE Visualization '94*, pages 248–254, 1994.

[16] P. Perona and J. Malik. Scale space and edge detection using anisotropic diffusion. In *IEEE Computer Society Workshop on Computer Vision*, 1987.

[17] T. Preußer and M. Rumpf. An adaptive finite element method for large scale image processing. In *Scale-Space Theories in Computer Vision*, pages 232–234, 1999.

[18] T. Preußer and M. Rumpf. Anisotropic nonlinear diffusion in flow visualization. In *Proceedings Visualization 1999*, 1999.

[19] H.-W. Shen and D. L. Kao. Uflic: A line integral convolution algorithm for visualizing unsteady flows. In *Proceedings Visualization '97*, pages 317–322, 1997.

[20] D. Stalling and H.-C. Hege. Fast and resolution independent line integral convolution. In *SIGGRAPH 95 Conference Proceedings*, pages 249–256. ACM SIGGRAPH, Addison Wesley, Aug. 1995.

[21] V. Thomée. *Galerkin - Finite Element Methods for Parabolic Problems*. Springer, 1984.

[22] J. J. van Wijk. Spot noise-texture synthesis for data visualization. In T. W. Sederberg, editor, *Computer Graphics (SIGGRAPH '91 Proceedings)*, volume 25, pages 309–318, July 1991.

[23] J. Weickert. *Anisotropic diffusion in image processing*. Teubner, 1998.